Dual faces of AREG in OSCC: Reduced circulating levels and enhanced tumor expression suggest compartmentalized regulation

NEHA KUMARI[1], CHARMI JYOTISHI[1], MANSI PATEL[2] and REESHU GUPTA[1,2]

[1]Parul Institute of Applied Sciences, Parul University, Vadodara, Gujarat 391760, India;
[2]Research and Development Cell, Parul University, Vadodara, Gujarat 391760, India

Received July 23, 2025; Accepted December 9, 2025

DOI: 10.3892/wasj.2025.421

Abstract. Oral squamous cell carcinoma (OSCC) remains a major global health concern due to its aggressive behavior and poor clinical outcomes, particularly in advanced, technically unresectable cases. The present study adopted a comprehensive multi-omics approach to identify potential biomarkers and therapeutic targets involved in the progression of OSCC. Differential gene expression analysis revealed 794 upregulated and 1,331 downregulated genes, with 16 genes significantly associated with both overall and disease-free survival. Among these, amphiregulin (*AREG*) and C-X3-C motif chemokine receptor 1 (*CX3CR1*) were identified through receiver operating characteristic analysis as the only two genes with a meaningful association with T4 tumor stage (*AREG*, upregulated; *CX3CR1*, downregulated), warranting further investigation. Epigenetic profiling revealed that copy number deletions and methylation changes in *CX3CR1* were linked to a decreased expression, supporting its tumor-suppressive role. By contrast, *AREG* exhibited upregulation despite Copy Number variation loss, suggesting additional regulatory influences, such as epigenetic or post-transcriptional mechanisms. Immune cell infiltration analysis demonstrated distinct associations of AREG with $CD8^+$ T-cells and CX3CR1 with neutrophils and $CD4^+$ T-cells, underscoring their role in tumor-immune interactions. Additionally, elevated DNA integrity ratios and the increased expression of AluY subfamilies were observed in patients with technically unresectable OSCC, suggesting a link between transposable element activity and tumor aggressiveness. Molecular docking and dynamics simulations further identified vinorelbine with high binding affinity for AREG, indicating its potential as therapeutic agents against OSCC. Taken together, these findings provide novel insight into the molecular landscape of OSCC and highlight *AREG, CX3CR1* and Alu elements as promising biomarkers for diagnosis and prognosis, as well as targets for future therapeutic interventions.

Correspondence to: Dr Reeshu Gupta, Research and Development Cell, Parul University, Post Limda, Waghodia Road, Vadodara, Gujarat 391760, India
E-mail: reeshu.gupta25198@paruluniversity.ac.in

Key words: oral squamous cell carcinoma, biomarkers, epigenetics, DNA methylation, Alu elements, immune infiltration, phytochemicals, molecular docking, targeted therapy

Introduction

Oral squamous cell carcinoma (OSCC) is an aggressive malignancy with high global incidence, particularly in Southeast Asia (1). Its tendency for late-stage diagnosis and early lymphatic spread contributes to poor outcomes, particularly in technically unresectable cases (2). While early-stage OSCC is associated with favorable survival rates, prognosis significantly exacerbates in advanced-stage disease (3,4). Identifying reliable molecular markers is crucial for early detection, prognostication and personalized treatment strategies. Recent advances in genomic and transcriptomic technologies have enabled the identification of differentially expressed genes (DEGs) associated with tumor growth, immune regulation and patient survival in OSCC (5). These molecular signatures provide valuable insight for early diagnosis, treatment stratification and monitoring therapeutic outcomes (6). In parallel, epigenetic alterations, such as DNA methylation and copy number variations (CNVs) are known to influence gene expression by silencing tumor suppressor genes or activating oncogenes, contributing to disease progression (7,8). The tumor microenvironment, particularly immune cell infiltration, also plays a critical role in shaping the clinical behavior of OSCC and influencing treatment response (9).

Transposable elements, such as Alu sequences contribute to genomic instability and have been implicated in cancer development through mechanisms such as insertional mutagenesis and RNA editing (10,11). Although typically found in introns, some Alu insertions can disrupt gene function by terminating transcription early (12,13). Furthermore, Alu sequences harbor multiple transcription factor binding sites, which can influence gene expression and potentially activate oncogenic pathways. Elevated fragmented Alu DNA in circulating DNA has been linked to a high tumor burden, suggesting their potential as non-invasive cancer biomarkers (14). Beyond standard

treatment approaches, there is growing interest in exploring phytochemicals and repurposed drugs as alternative means to interfere with oncogenic signaling in OSCC. Naturally occurring compounds derived from plants have demonstrated anticancer activity and are valued for their potential to reduce toxicity, while inhibiting tumor progression (15). At the same time, established chemotherapeutic agents, such as vinorelbine are being reconsidered for new applications, particularly through the analysis of their binding affinity to cancer-related molecular targets. *In silico* techniques, such as molecular docking and molecular dynamics simulations currently play a key role in predicting and validating the therapeutic relevance of these candidate compounds (16).

The present study focused on combining genomic, epigenetic, immunological and transposable element analyses to uncover key biomarkers and therapeutic targets associated with OSCC. Gaining insight into the molecular events that drive OSCC progression can support the advancement of precision medicine strategies and enable the development of biomarker-guided interventions, with the goal of enhancing early diagnosis, prognostic accuracy and treatment outcomes.

Materials and methods

Analysis of DEGs. The analysis was performed using RNA sequencing data from the Gene Expression Omnibus (GEO) database for oral cancer (GSE246050). DEGs were identified using GEO2R, an interactive tool for analyzing high-throughput gene expression data. The DEGs were identified based on the criteria of a log fold change (LogFC) of ≥1 for upregulated genes and <-1 for downregulated genes. Genes meeting these thresholds and exhibiting a false discovery rate (FDR)-adjusted P-value ≤0.05 were deemed statistically significant (17).

Interaction network construction. The protein-protein interaction (PPI) network of DEGs was constructed using the STRING database. To further analyze the network, the list of genes was imported into Cytoscape (version 3.9.1) for the visualization and topological analysis of the structural properties of the network. A high-confidence interaction score (≥0.7) was applied to assess the degree of connectivity within the network. Key hub genes were identified based on a degree threshold of ≥10, indicating their central role in the interaction network.

Survival analysis and heatmap visualization of the survival associated genes. The overall survival (OS) and disease-free survival (DFS) analyses of genes from the GEO dataset were performed using the Gene Expression Profiling Interactive Analysis (GEPIA) online tool (18), which has been cited in >400 studies (19). GEPIA performs a survival analysis on the basis of the gene expression level, and a hypothesis is evaluated using the log-rank test (Mantel-Cox test). Hazard ratios (HR) were calculated using the Cox proportional hazards model with 95% confidence intervals (CIs). Genes that had a log-rank P-value of ≤0.05 were regarded as significant. To visualize the expression pattern of these important genes heatmap was created using the Complex Heatmap package in R studio (20).

cBioPortal analysis. To assess the impact of survival-related DEGs on patient outcomes, the expression data of head and neck squamous cell carcinoma (HNSCC) were downloaded from the Firehose Legacy dataset of cBioPortal (https://www.cbioportal.org/datasets). The dataset contained the American Joint Committee on Cancer (AJCC) pathological staging, survival data, patient IDs and gene expression values. Gene expression values were categorized as high or low based on the median ± 2SEM cut-off. The receiver operating characteristic (ROC) curve analysis was conducted to identify the prognostic value of the selected genes in relation to OS using survival duration in months and dichotomized levels of gene expression (high and low). Genes with a greater area under the curve (AUC) were regarded as having a greater predictive potential and were selected to be further analyzed. Moreover, the ROC analysis was also utilized to examine the association between the patterns of gene expression and the advanced T4 tumor stage classification, which also provides information about their association with the severity of the disease. OriginPro (version 2019b; https://www.originlab.com/) was used all statistical analysis since it offers advanced statistical analysis tools to enable comprehensive analysis of data. ROC curves were generated based on a classification model at all classification thresholds, incorporating true positive rate (sensitivity) and false positive rate (1-specificity) as key parameters. A P-value <0.05 was considered to indicate a statistically significant difference.

Gene Ontology (GO) and pathway analysis. Functional enrichment analysis was performed using the WEB-based GEne SeT AnaLysis Toolkit (WebGestalt; https://www.webgestalt.org/), which includes GO annotation and Kyoto Encyclopedia of Genes and Genomes (KEGG) pathway analysis (21).

Association of selected genes with methylation probes. The methylation profiling of selected genes was conducted using the MethSurv database, which enables CpG site-specific survival analysis based on methylation level (22). The platform performs univariable and multivariable survival analyses for CpG sites located within or near the query gene using Cox proportional hazards models. Differences in survival between highly methylated and lowly methylated patient groups are visualized using Kaplan-Meier (KM) plots.

CNV and gene expression correlation analysis. To validate the correlation between CNVs and survival-associated DEGs in an independent cohort, RNA sequencing data from The Cancer Genome Atlas (TCGA) were accessed via cBioPortal (http://www.cbioportal.org). CNV data were pre-processed using Genomic Identification of Significant Targets in Cancer (GISTIC), which estimates somatic copy number alterations for each annotated gene. The CNV values were categorized as follows: -2 (homozygous deletion), -1 (heterozygous loss), 0 (diploid), 1 (single-copy gain), and 2 (high-level amplification or multiple-copy gain). A Spearman's correlation analysis was conducted to determine the correlation between CNVs and the level of gene expression using a linear regression model. The Rho values of Spearman's correlation were used to evaluate the correlation.

Table I. Clinical and pathological characteristics of the patients and controls included in the present study.

Group	Age (years)	Sex	Stage/substage	Sample type	HIV status	HCV status
OSCC	65	Female	CT2aN1M0	Blood	Positive	Non-reactive
OSCC	58	Male	CT4aN1M0	Blood	Positive	Non-reactive
OSCC	72	Male	CT1aN1M0	Blood	Information not available	Information not available
OSCC	62	Male	CT4aN1M0	Blood	Positive	Non-reactive
OSCC	62	Male	CT2aN1 M0	Blood	Positive	Non-reactive
OSCC	32	Male	CT2aN1 M0	Blood	Information not available	Information not available
OSCC	49	Female	CT2aM0	Blood	Information not available	Information not available
OSCC	42	Male	CT4aM0	Blood	Information not available	Information not available
OSCC	52	Female	CT2aN1	Blood	Positive	Non-reactive
TUOC	62	Male	CT1aN1M0	Blood	Information not available	Information not available
TUOC	39	Female	CT4aN1M0	Blood	Information not available	Information not available
TUOC	53	Male	CT2aN2M0	Blood	Information not available	Information not available
TUOC	42	Female	CT4aN2M0	Blood	Positive	Information not available
TUOC	45	Male	CT4aN2M0	Blood	Positive	Non-reactive
TUOC	44	Male	CT4aN2M0	Blood	Positive	Non-reactive
TUOC	43	Female	CT2aN2M0	Blood	Positive	Non-reactive
TUOC	67	Male	CT1aM0	Blood	Positive	Non-reactive
TUOC	57	Female	CT2aN2	Blood	Positive	Non-reactive
Control	24	Female	-	-	-	-
Control	27	Female	-	-	-	-
Control	23	Female	-	-	-	-
Control	24	Female	-	-	-	-
Control	23	Male	-	-	-	-
Control	23	Male	-	-	-	-

OSCC, oral squamous cell carcinoma; TUOC, technically unresectable oral cancer; HIV, human immunodeficiency virus; HCV, hepatitis C virus.

Correlation between amphiregulin (AREG) and C-X3-C motif chemokine receptor 1 (CX3CR1) and immune infiltration. The association between *AREG* and *CX3CR1* expression and tumor-infiltrating immune cells was analyzed using the TIMER 2.0 database (http://timer.comp-genomics.org/) (23). The infiltration scores were calculated using the single-sample Gene Set Enrichment Analysis (ssGSEA) method. Additionally, heatmaps were generated to visualize the correlation between the expression of genes and the immune cell infiltration based on Spearman's Rho values. The analysis provides the understanding of the possible role of the survival-related DEGs in immune modulation in the tumor microenvironment.

Patients and ethics statement. The present study enrolled 18 patients from Parul Sevashram Hospital, Vadodara, India, including 9 patients with oral cancer and 9 patients with technically unresectable oral cancer (TUOC). The study protocol was reviewed and approved by the Ethics Committee of Parul University (Approval no. PUIECHR/PIMSR/00/081734/5307) and was conducted in accordance with institutional ethical standards and regulatory guidelines. All patients signed an informed consent form. In addition, blood samples were collected from 6 healthy individuals to serve as controls for the DNA-based assays (Table I). All procedures performed in the present study were in accordance with the principles for medical research of the 1964 Declaration of Helsinki and its later amendments or comparable ethical standards.

Patient cohort. The clinical and pathological details of all patients included in the study are summarized in Table I. The table provides information on age, sex, tumor stage, grade, tumor size, lymph node status and HIV results. In the OSCC group, the age of the patients ranged from 32 to 72 years, with a median age of 58±4.18 years. In the TUOC group, the age ranged from 39 to 67 years, with a median age of 45±3.30 years. Data on HCV status were not available for all cases, as this information was not routinely recorded in patient files. Since the study focused primarily on gene expression profiling rather than viral-associated carcinogenesis, the absence of HCV data does not affect the interpretation of the findings (24).

Reverse transcription-quantitative polymerase chain reaction (RT-qPCR). Total RNA was extracted from fresh blood using the QIAamp® RNA Blood Mini kit (cat. no. 52304; Qiagen, Inc.) and RNA purity was confirmed by spectrophotometric analysis (A260/A280 ratio between 1.8-2.0). cDNA was synthesized from 20 ng RNA using the G-Biosciences cDNA Synthesis kit (cat. no. 786-5020; G-Biosciences) and used

for qPCR on the Rotor-Gene Q system with SYBR-Green Master mix (cat. no. 786-5062; G-Biosciences). qPCR was run in triplicate under standard cycling conditions as follows: 95˚C for 3 min, followed by 40 cycles of 95˚C for 15 sec and 60˚C for 60 sec. The relative expression levels of the target gene mRNAs were calculated using the comparative Cq method (relative expression, $2^{-\Delta\Delta Cq}$) (25), using GAPDH as an internal control. The primer sequences were as follows: *AREG* forward, 5'-GTGGTGCTGTCGCTCTTGATACTC-3' and reverse, 5'-TCAAATCCATCAGCACTGTGGTC-3'; C*X3CR1* forward, 5'-GGGACTGTGTTCCTGTCCAT-3' and reverse, 5'-GACACTCTTGGGCTTCTTGC-3'; and *GAPDH* forward, 5'-CCCACTCCTCCACCTTTGAC-3' and reverse, 5'-TTC CTCTTGTGCTCTTGCTG-3'.

Alu DNA quantification. Blood DNA was extracted from patients with 18 oral cancers using the QIAamp DNA Blood Mini kit (cat. no. 51104; Qiagen, Inc.) and stored at -80˚C. AluY sequences and subtypes were obtained from the Dfam database (26), and qPCR was conducted in triplicate using primers for AluY, (forward, 5'-GTAATCCCAGCACTT TGGG-3' and reverse, 5'-TAGTAGAGACGGGGTTTCAC-3'), AluY-K12 (forward, 5'-TACAAAAAATTAGCCGGGCG-3' and reverse, 5'-CATGCCATTCTCCTGCCTC-3' and AluY-I6 (forward, 5'-GTAATCCCAGCACTTTGGG-3' and reverse, 5'-GTTCACGCCATTCTCCTGC-3'). Each 10 μl PCR reaction consisted of 5 μl SYBR-Green mix (G-Biosciences), 1 μl forward/reverse primer (10 μM), and 100 pg DNA. The cycling conditions were 95˚C for 10 min, followed by 45 cycles at 95˚C for 15 sec and 60˚C for 60 sec, and a hold at 60˚C for for ALUY and ALUY-K12. For ALUY-I6, the conditions were 95˚C for 10 min, 30 repeats at 95˚C for 15 sec, and 65˚C for 60 sec. The specificity of the PCR products was confirmed by melting curve analysis. The specificity of the PCR products was confirmed by melting curve analysis. Quantification of total blood Alu DNA content was based on a standard curve prepared from serial dilutions of genomic DNA (10 ng to 0.01 pg) from healthy donors. Each qPCR run included a no-template control, and the results are reported as the mean ± SEM.

Molecular docking analysis of AREG inhibitors. A library of 1,525 plant-derived bioactive compounds was initially screened using SWISS-ADME to evaluate their physicochemical properties and drug-likeness, resulting in the selection of 174 potential candidates. In parallel, 50 clinically reported anticancer drugs were shortlisted based on literature evidence for their relevance in cancer therapy. Molecular docking was performed between these compounds and the AREG protein using PyRx, with the AREG structure obtained from PDB (2RNL) and compound structures retrieved from PubChem (27). Among the screened molecules, the top two compounds exhibiting the highest binding affinity and key hydrogen bonding interactions with AREG were selected for molecular dynamics simulations to further assess their stability and inhibitory potential.

Molecular dynamics simulations. Molecular dynamics simulations were carried out for cabraleadiol (CID-21625899) and vinorelbine in complex with AREG using the NAMD3 simulation package with the CHARMM force field. Key structural parameters, including root mean square deviation (RMSD), root mean square fluctuation (RMSF) and radius of gyration (Rg), were calculated using NAMD3 system-building commands and visualized with the Bio3D v2.3-0 package (http://thegrantlab.org/bio3d_v2/download). The simulation was run for a total of 200 nsec, and the binding free energy (ΔG) of each drug-protein complex was estimated using the NAMD Energy plugin.

Statistical analysis. The expression of DEGs in GEO2R was assessed using moderated t-tests with the Benjamini-Hochberg FDR correction ($|LogFC| \geq 1$). Survival analyses were conducted in GEPIA using Cox proportional hazards models and log-rank tests, with HRs and 95% CIs reported. ROC curves (OriginPro 2019b) were generated using survival duration and dichotomized gene expression, and AUC values assessed prognostic performance. Spearman's correlation analysis was used to analyze the correlations between CNV and gene expression and immune infiltration scores in TIMER 2.0. MethSurv applied Cox regression to compare survival between high- and low-methylation groups. qPCR data from the three study groups (resectable oral cancer, n=9; technically unresectable oral cancer, n=9; and healthy controls, n=6) were analyzed using the $2^{-\Delta\Delta Cq}$ method and are presented as the mean ± SEM. Comparisons among the three groups were performed using one-way ANOVA, followed by Tukey's post hoc test to identify pairwise differences. Alu DNA quantification was performed on two groups (resectable oral cancer vs. technically unresectable oral cancer; n=9 per group) and compared using an unpaired two-tailed Student's t- test. For all analyses, a P-value <0.05 was considered to indicate a statistically significant difference. All statistical analyses were performed using OriginPro 2019b (https://www.originlab.com/).

Results

Identification of prognostic biomarkers in OSCC using integrated bioinformatics analysis of GEO datasets. A total of 20,030 genes were identified from the GSE246050 dataset using GEO2R analysis. Among these, 794 genes were significantly upregulated and 1,331 were downregulated in the OSCC samples compared to the healthy controls. To focus on the most relevant molecular interactions, only genes with an interaction degree of ≥10 in Cytoscape were retained for further analysis. This filtering step yielded 318 upregulated and 221 downregulated genes (Table SI), which were then subjected to survival analysis using GEPIA. Among the upregulated genes, 46 exhibited a significant association with OS, 28 with DFS, and six genes were linked to both OS and DFS. Similarly, among the downregulated genes, 41 genes were associated with OS, 24 with DFS, and ten genes displayed significance in both categories (Table SII). Heatmap analysis of genes affecting both OS and DFS revealed six upregulated genes (*ACTB, HPRT1, PPIA, MAD2L2, AREG, ADORA2B*) and ten downregulated genes (*MFAP4, ALDH3A1, CX3CR1, ERVW-1, CYP4A11, PLA2G3, LRRK2, NTRK2, CACNA2D4, KL*), as shown in Fig. 1. These differentially expressed genes, which affect

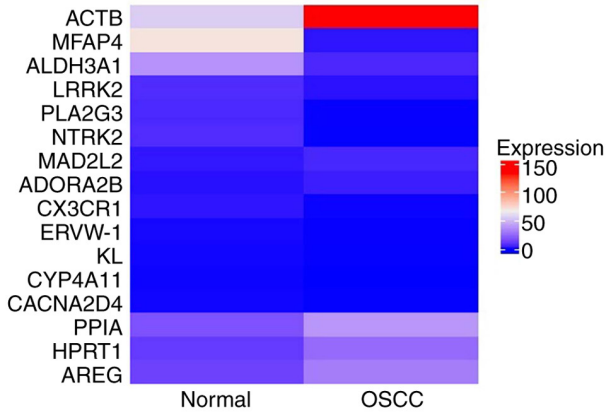

Figure 1. Heatmap analysis of genes affecting both overall survival and disease-free survival in oral cancer. OSCC, oral squamous cell carcinoma.

both OS and DFS, were identified as potential survival-associated biomarkers for further investigation.

GO and KEGG pathway enrichment analysis of 16 survival-associated genes. GO functional enrichment and KEGG pathway analyses were used to examine the biological functions and molecular pathways of genes related to both OS and DFS. Enriched GO terms were categorized into three groups, including biological process (BP), cellular component (CC) and molecular function (MF) (Table SIII). Under the BP category, key terms such as phosphorylation, cell activation and leukocyte-mediated immunity were identified, which suggests their involvement in immune response and cellular signaling. The CC category featured the enrichment of presynapse, axon terminus, neuron projection terminus and elastic fibers, suggesting that they are involved in neural signaling and extracellular matrix organization. Among the enriched terms in the MF category, G-protein coupled receptor activity, chemokine binding, growth factor binding, and fatty acid hydroxylase activity were identified, indicating the variety of functions in the process of signal transduction and metabolism. In addition, KEGG pathway enrichment analysis revealed several signaling pathways related to the target genes (Table SIV). These were the MAPK signaling pathway, which is crucial in cell proliferation and survival, the oxytocin signaling pathway, which is involved in cellular communication and immune regulation, the Hippo signaling pathway, which controls the size of the organs and cell growth, and the pathways of bacterial invasion of epithelial cells, which suggests its potential implication in infection-associated oncogenesis. These results provide information on the functional role of the identified genes and their role in the key oncogenic and immune control pathways.

Validation of selected genes in the cBioPortal database. The Head and Neck Squamous Cell Carcinoma (TCGA, Firehose Legacy) dataset was obtained from cBioPortal, and RSEM expression data for genes associated with both OS and RFS were extracted. Among the ten identified downregulated genes, only seven (excluding *ERVW-1, LRRK2* and *KL*) were available in the cBioPortal dataset. All gene expression data were analyzed to determine RSEM cut-off values for classifying high and low expression levels for each gene. Patients were stratified into high- and low-risk groups based on the cut-off value, determined as the median ± 2SEM of gene expression level and on the basis of their impact on overall survival. Out of the 13 genes initially identified through survival analysis using cBioPortal data, seven genes (*ACTB, AREG, HPRT1, MFAP4, ALDH3A1, CYP4A11* and *CACNA2D4*) demonstrated statistically significant associations with either OS, RFS, or both, indicating their potential as prognostic markers in OSCC (Table II). Further evaluation through ROC curve analysis revealed that only *AREG, HPRT1*, *ALDH3A1* and *CX3CR1* had an AUC ≥0.60, suggesting their moderate diagnostic value (Figs. 2 and 3). To assess the relevance of these four genes in advanced disease, ROC analysis was performed using T4-stage classification. Among the candidate genes, *AREG* (upregulated) and *CX3CR1* (downregulated) exhibited the highest AUC values (~0.6), indicating relatively better discrimination of advanced-stage OSCC compared to the others (Fig. 4). Although their overall diagnostic performance was moderate, their stage-specific expression trends and biological links to tumor progression and immune regulation supported their selection for detailed downstream analysis (28-30).

Association of AREG and CX3CR1 with methylation probes. According to methylation profile data from the MethSurv database, *AREG* is associated with five specific methylation probes: cg02009651, cg03244277, cg02334660, cg26611070 and cg15529290 (Fig. 5). Among these, methylation levels at CpG sites cg02009651, cg03244277 and cg15529290 were negatively associated, whereas methylation at cg02334660 and cg26611070 was associated with a favorable prognosis correlation. Additionally, the analysis of the association between these CpG sites and demographic/clinical factors including ethnicity, race, body mass index (BMI), age and clinical events revealed that cg02334660 and cg26611070 were positively association with these variables, while cg15529290 (at 1st exon), cg02009651 and cg03244277 exhibited a negative association.

From the *CX3CR1* methylation profile data from the MethSurv database, *CX3CR1* was shown to be associated with 11 specific methylation probes: cg24130739, cg03296370, cg19838154, cg01394385, cg26162331, cg00262061, cg05046858, cg04498110, cg04569233, cg03341377 and cg24310395 (Fig. 6). Methylation-survival analyses were performed using the MethSurv web tool, which fits Cox proportional hazards models and reports hazard ratios, log-rank test p-values, and a proportional hazards assumption test for each CpG site (22). The log-rank test has optimum power under the assumption of proportional hazard rates. However, this assumption is often violated, particularly when two survival curves cross each other. In Fig. 6, the late crossing of the survival curve can be observed in the last plot. The authors were not able to restrict the time range in the software to remove the late-stage crossover. In addition, survival analyses for methylation were obtained from the MethSurv platform using aggregate output; thus, the application of alternative weighted tests was not possible. Therefore, this may be a limitation of the present study. Among these, methylation levels at cg24130739, cg03296370, cg19838154, cg03341377, CpG sites were negatively associated, whereas methylation at cg00262061, cg04498110, cg03341377,

Table II. Survival analysis of the survival-associated DEGs identified in oral cancer from the cBioPortal database.

Gene symbol	Risk status (no. of patients)	Survival/deceased status (no. of patients)	P-value	DFS/RFS (no. of patients)	P-value
Upregulated genes					
ACTB	High risk (245)	OS (129); Deceased (116)	0.0062[a]	DFS (108); Recurred (73)	2.9662
CO:139086.35±130633.33	Low risk (242)	OS (157); Deceased (85)		DFS (131); Recurred (61)	
AREG	High risk (234)	OS (121); Deceased (113)	0.0319[a]	DFS (97); Recurred (76)	0.0067[a]
CO:789.911±514.86	Low risk (234)	OS (144); Deceased (90)		DFS (124); Recurred (53)	
HPRT1	High risk (244)	OS (121); Deceased (123)	0.0001[a]	DFS (97); Recurred (74)	0.0071[a]
CO:964.36±884.77	Low risk (238)	OS (159); Deceased (79)		DFS (135); Recurred (57)	
PPIA	High risk (235)	OS (132); Deceased (103)	0.3980	DFS (109); Recurred (73)	0.2849
	Low risk (218)	OS (131); Deceased (87)		DFS (108); Recurred (57)	
MAD2L2	High risk (234)	OS (127); Deceased (107)	0.2077	DFS (104); Recurred (74)	2.1575
CO:743.67±656.76	Low risk (240)	OS (144); Deceased (96)		DFS (120); Recurred (62)	
ADORA2B	High risk (243)	OS (132); Deceased (111)	0.1296	DFS (107); Recurred (76)	0.7371
CO:429.28±377.05	Low risk (227)	OS (139); Deceased (88)		DFS (117); Recurred (56)	
Downregulated genes					
MFAP4 CO:373.16±166.62	High risk (211)	OS (131); Deceased (80)	0.0363[a]	DFS (112); Recurred (49)	0.0062[a]
	Low risk (195)	OS (101); Deceased (94)		DFS (80); Recurred (67)	
ALDH3A1	High risk (197)	OS (118); Deceased (79)	0.0054[a]	DFS (99); Recurred (46)	0.0312[a]
CO:2152.11±184.34	Low risk (94)	OS (40); Deceased (54)		DFS (32); Recurred (29)	
CX3CR1	High risk (232)	OS (138); Deceased (94)	0.4080	DFS (119); Recurred (58)	2.9959
CO:25.29±16.56	Low risk (214)	OS (119); Deceased (95)		DFS (96); Recurred (69)	
CYP4A11, CO:0.55±0.20	High risk (201)	OS (135); Deceased (66)	0.0026[a]	DFS (116); Recurred (47)	0.0074[a]
	Low risk (227)	OS (120); Deceased (107)		DFS (97); Recurred (73)	
PLA2G3,	High risk (220)	OS (133); Deceased (87)	0.1919	DFS (116); Recurred (51)	3.4236
CO:140.43±66.95	Low risk (212)	OS (115); Deceased (97)		DFS (93); Recurred (63)	
NTRK2	High risk (210)	OS (126); Deceased (84)	0.1103	DFS (106); Recurred (50)	0.0378[a]
CO:1166.69±98.61	Low risk (103)	OS (52); Deceased (51)		DFS (41); Recurred (35)	
CACNA2D4	High risk (233)	OS (145); Deceased (88)	0.0398[a]	DFS (123); Recurred (62)	0.1449
CO:24.26±19.58	Low risk (222)	OS (117); Deceased (105)		DFS (93); Recurred (65)	

OS, overall survival; DFS, disease-free survival; CO, cut-off value. [a]P≤0.05, indicates a significant difference.

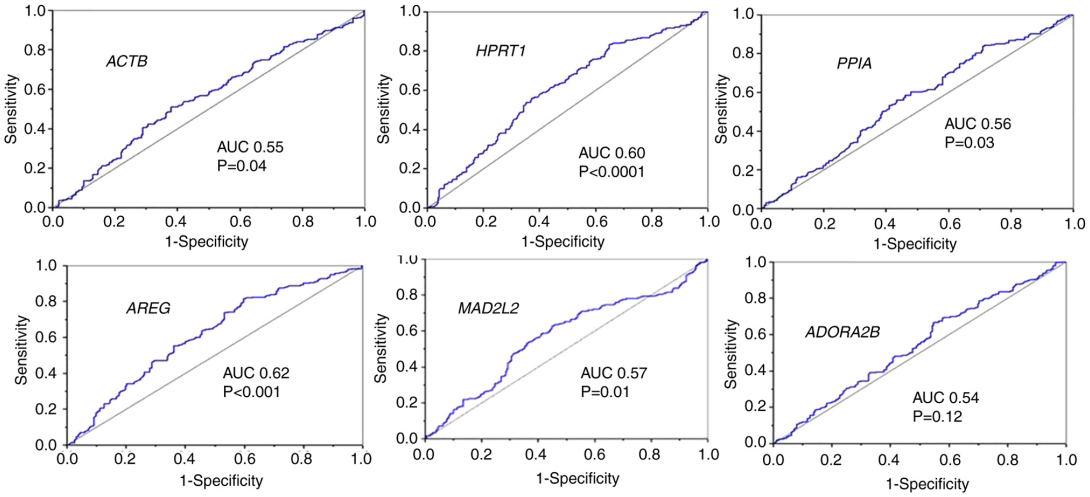

Figure 2. Receiver operating characteristic analysis of upregulated genes affecting both overall survival and disease-free survival in oral cancer. AUC, area under the curve.

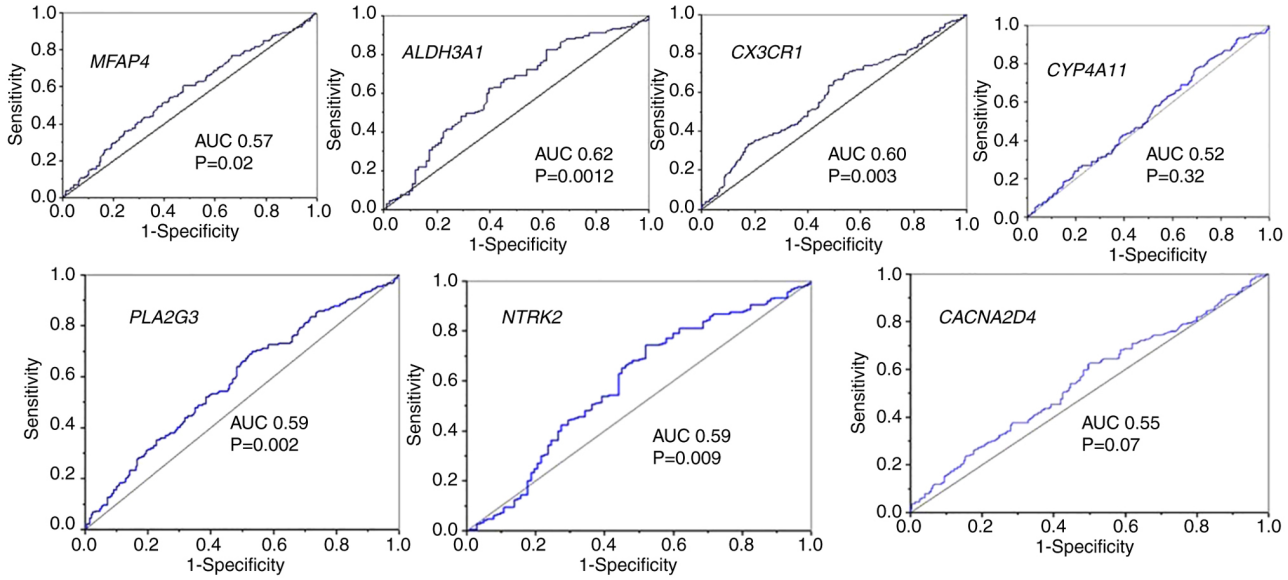

Figure 3. Receiver operating characteristic analysis of downregulated genes affecting both overall survival and disease-free survival in oral cancer. AUC, area under the curve.

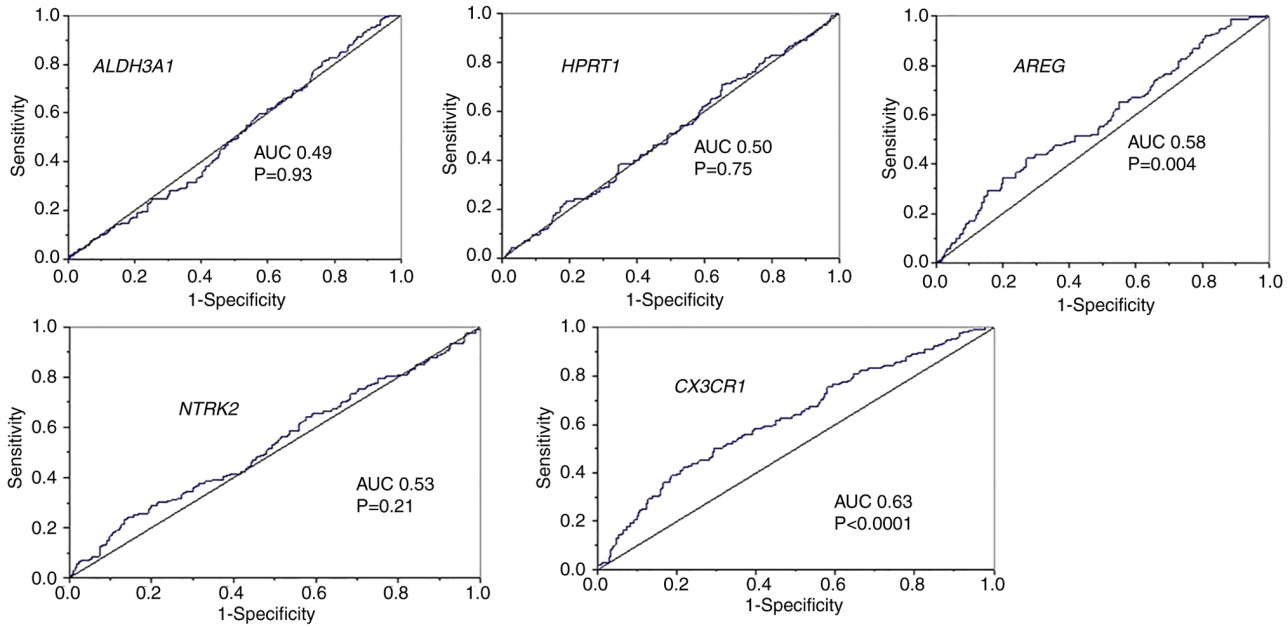

Figure 4. Receiver operating characteristic analysis of ALDH3A1, HPRT1, AREG, NTRK2, and CX3CR1 genes in relation to tumor stages in oral cancer.

cg24310395, cg04569233, cg05046858 and cg26162331 was associated with a favorable prognosis. Additionally, the analysis of the association between these CpG sites and demographic/clinical factors, including ethnicity, race, BMI, age and clinical events revealed that methylation at cg01394385, cg26162331, cg00262061 and cg05046858 were positively associated with these variables, while methylation at cg24130739, cg03296370, cg19838154, cg04498110, cg04569233, cg03341377 and cg24310395 exhibited a negative association (Fig. 6).

Copy number analysis. CNV is known to influence gene expression; however, the association between CNVs of *AREG* and *CX3CR1* and their impact on gene expression in oral cancer remain to be fully elucidated. Correlation analysis was performed using the HNSCC dataset hosted on cBioPortal, based on patients with paired copy-number and expression data (AREG, n=234; CX3CR1, n=524). In the present study, the analysis revealed a significant effect of CNV on gene expression (P<0.001; (Fig. 7). From a tumor biology perspective, GISTIC2 analysis identified significant CNV events, which may contribute to the observed differences in gene expression. To further investigate this association, patients were stratified into high- and low-risk groups based on a cut-off value determined as the median ± SEM of gene expression levels. CNV analysis revealed that copy number

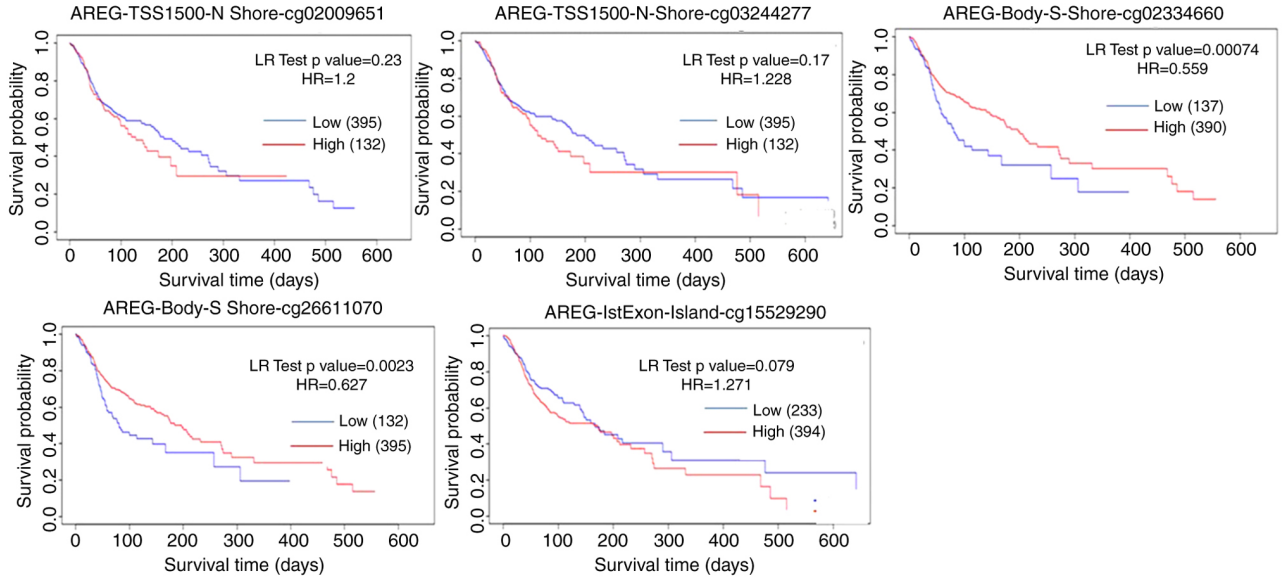

Figure 5. Association of AREG methylation on survival outcomes in oral cancer.

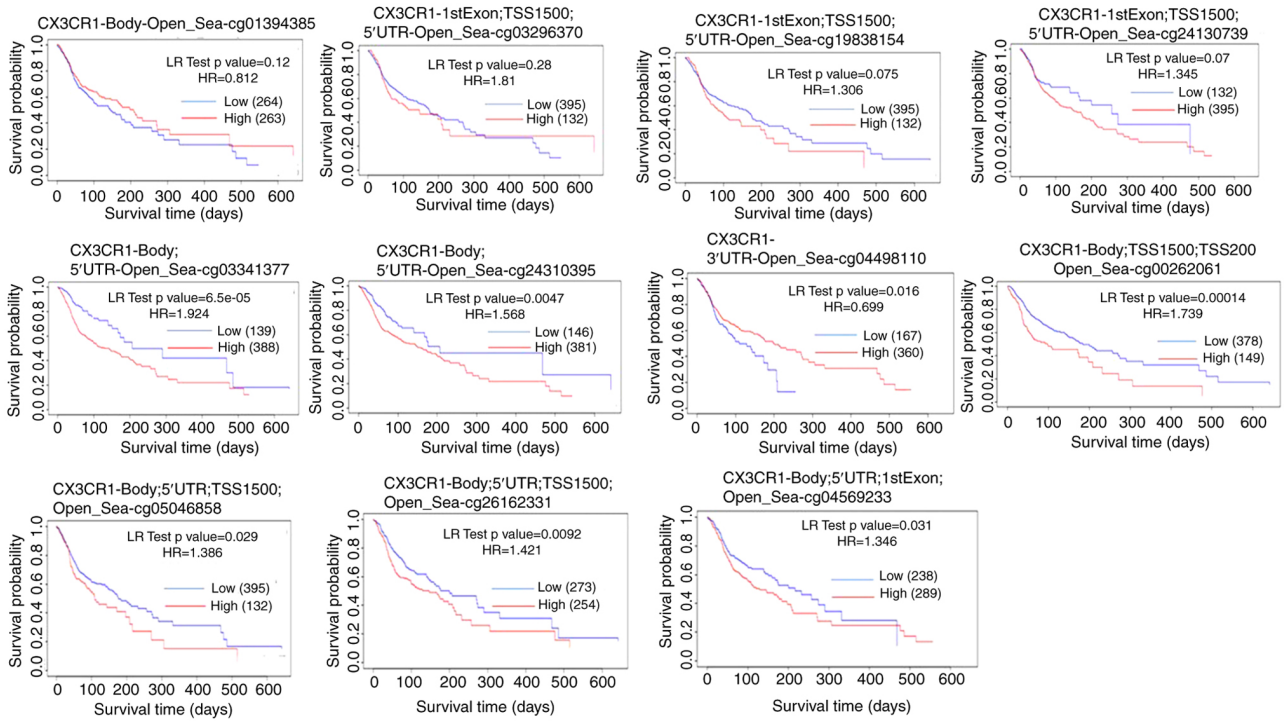

Figure 6. Association of CX3CR1 methylation on survival outcomes in oral cancer.

deletions were significantly associated with a decreased gene expression of both *AREG* (high, 35/230; low, 71/232; P=0.000137) and *CX3CR1* (high, 142/227; low, 163/213; P=0.0058) in the cBioPortal dataset for HNSCC. However, no significant differences were observed for copy number amplifications (Table III).

To further validate the correlations between CNV and gene expression, a linear regression model was applied using HNSCC data from cBioPortal. The analysis revealed a weak correlation between gene expression and copy number alterations for both AREG (ρ=0.213, P=0.00098) and CX3CR1 (ρ=0.159, P=0.00029), as shown in Fig. 7A and B. Although the correlation coefficients indicate weak associations, they are statistically significant due to the large sample size.

AREG and CX3CR1 expression are associated with immune cell infiltration. The results of TIMER analysis suggested that *AREG* and *CX3CR1* exhibit differential immune infiltration patterns in HNSCC. Notably, *CX3CR1* appears to be more strongly associated with neutrophil and $CD4^+$ T-cell infiltration, while *AREG* is associated more with $CD8^+$ T-cells (Fig. 8). These findings may provide insight into the

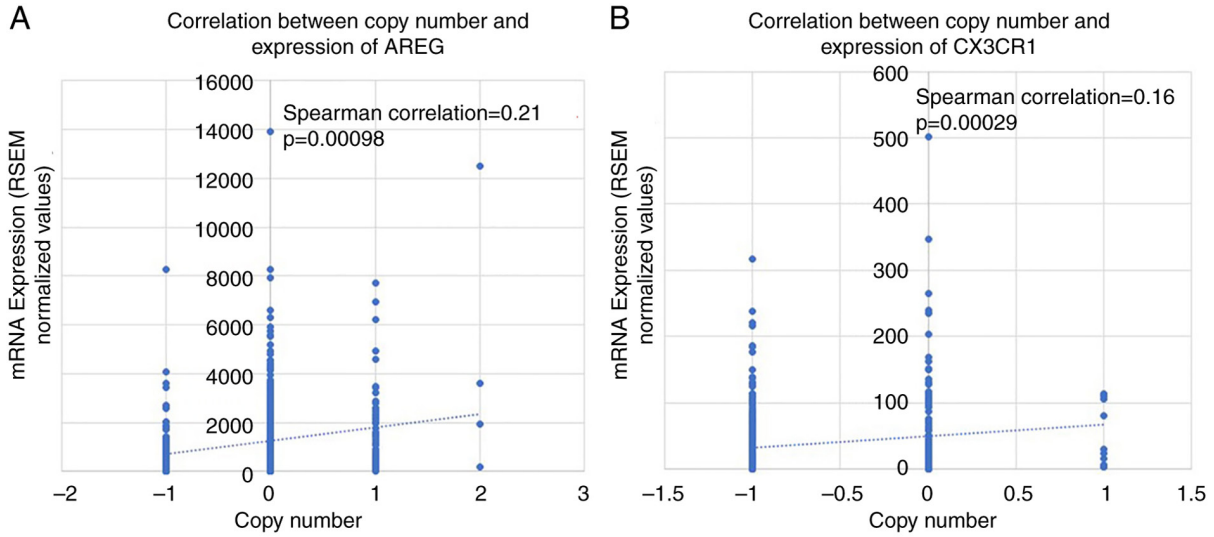

Figure 7. Spearman's correlation analysis of (A) AREG and (B) CX3CR1 gene expression and copy number alterations.

Table III. Distribution of *AREG* and *CXC3CR1* copy number alterations in the high- and low-expression groups.

	Deletion	No change	Amplification	Total
AREG				
High	35	155	40	230
Low	71	138	23	232
CX3CR1				
High	142	80	5	227
Low	163	46	4	213

immunomodulatory roles of these genes in the HNSCC tumor microenvironment.

RT-qPCR analysis of AREG and CX3CR1 in oral cancer. Subsequently, the expression levels of *AREG* and *CX3CR1* were evaluated in the blood samples of patients with oral cancer. *AREG* expression was found to be reduced in technically unresectable cases (TUOC, 0.16-fold change ± 0.08) compared to patients with resectable cancer (0.39-fold change ± 0.15) (Fig. 9). By contrast, *CX3CR1* expression could not be reliably detected, as its Cq value was >42, indicating levels below the measurable limit.

Phytochemicals as AREG potential inhibitors. Of the 1,525 phytochemicals screened, 274 displayed drug-like properties, indicating potential as drug candidates. Similarly, Gene Set Cancer Analysis (GSCA) identified 84 inhibitors for AREG by co-relating drug sensitivity and gene expression. Binding affinity scores were calculated for both 274 phytochemicals and 84 AREG inhibitors. The (25s)-neospirost-4-en-3-one for phytochemical and vinorelbine for inhibitors demonstrate highest binding affinity to AREG and therefore, were prioritized for binding energy calculation. The list of top 20 phytochemicals and inhibitors is presented in Tables IV and V, respectively.

Molecular docking and molecular dynamics simulation. Docking analysis revealed the highest binding affinity between AREG- (25s)-neospirost-4-en-3-one and AREG-vinorelbine (Tables IV and V).

The stability and compactness of these complexes were assessed through RMSD and radius of gyration (Rg), as demonstrated in Table VI and Fig. 10. The RMSD and Rg did not fluctuate for the 200 nsec, confirming the stability of the 3D protein structure during molecular dynamics simulations. Additionally, the RMSF was stable over 200 ns of simulation, suggesting least residue-level fluctuations. These findings strongly support the stable interaction of the complexes during the 200 nsec simulation, confirming their structural stability and potential effectiveness.

The results also revealed that the binding energy between AREG-vinorelbine was -15.26 kcal/mol, while the binding energy between AREG- (25s)-neospirost-4-en-3-one was +3.6 kcal/mol (Table VII). These results suggest a strong binding interaction of vinorelbine with AREG in comparison to (25s)-neospirost-4-en-3-one.

Analysis of Alu family expression in patients with oral cancer and TUOC. In the present study, Alu DNA levels were quantified in serum samples from patients with resectable oral cancer and TUOC to evaluate their potential as biomarkers. The DNA integrity (DI) ratio, measured using Alu115/Alu247, was significantly elevated in patients with TUOC (16.46±3.82) compared to patients with resectable OSCC (0.55±0.11), with a P-value of 0.0007, indicating increased genomic instability in advanced-stage disease (Fig. 11). The analysis of AluY subfamilies revealed a non-significant increase in AluY (K12) expression in patients with TUOC (0.43±0.22) vs. patients with resectable OSCC (0.11±0.03; P=0.1715), and a similar trend was observed for AluY (i6) (TUOC, 1.44±0.25; resectable OSCC, 1.27±0.29; P=0.6589) (Fig. 11). Of note, total AluY family expression, encompassing all subtypes, was significantly higher in patients with resectable OSCC (6.83±1.83) than in those with TUOC (1.60±0.51; P=0.0143) (Fig. 11). These results suggest that while individual AluY subfamilies

Table IV. List of top 20 phytochemical inhibitors demonstrating binding affinity scores and hydrogen bond interactions.

Name	Binding affinity	Hydrogen bonds
(25s)-neospirost-4-en-3-one	-7.5	TYR-27
Limonin	-7.1	ASN-10, LYS-26
2-(4-hydroxyphenyl) naphthalic anhydride	-6.7	TYR-27
Cucurbita-5_23(e)-diene-3-beta_7-beta_25-triol	-6.7	HIS-30, LYS-9
Betulinic_acid	-6.7	LYS-9
Caloxanthone_a	-6.7	LYS-9
Garcimangosxanthone_b	-6.7	GLN-17
2_3-dihydrowithaferin_a	-6.6	CYS-38, LYS-37
Garcidepsidone_b	-6.6	TYR-27, GLU-15
3-beta-acetoxy-8-beta-isobutyryloxyreynosin	-6.5	TYR-27
8-prenyl_erythrinin_c	-6.5	TYR-42, GLN-39, CYS-38, LYS-37
Caloxanthone_a	-6.5	LYS- 9, GLU-15
Eichlerialactone	-6.5	LYS-26
Garcimangosxanthone_c	-6.5	GLY-17, CYS-25, GLY-23
3-beta__12-dihydroxy-13-methyl-6_8_11_13-podocarpatetraen	-6.4	TYR-27, ASN-10 GLY-7, LYS-26
Metrhylmitrekaurenate	-6.3	TYR-27
Xanthone V1	-6.3	LYS-9, GLU-32 TYR-27, GLU-29
Escobarine A	-6.2	GLY-7, LYS-9 TYR-27
Garcidepsidone A	-6.2	TYR-27
2r_3r)-3_5-dihydroxy-7-methoxy_avanone	-6.1	TYR-27

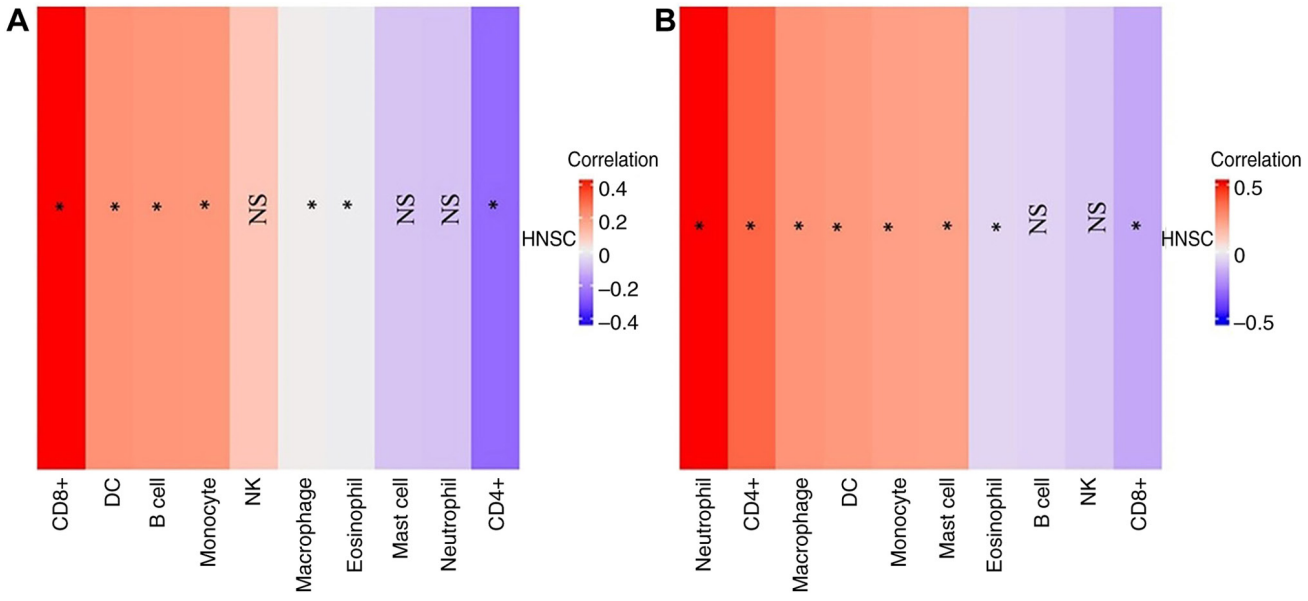

Figure 8. Correlation analysis of (A) AREG and (B) CX3CR1 expression and immune infiltration. *P<0.05; NS, not significant (P>0.05).

may not distinctly reflect disease stage, elevated DI ratios and changes in total AluY expression may serve as potential indicators of disease progression and early-stage tumor activity in OSCC.

Discussion

OSCC is an aggressive malignancy and has low chances of survival because of late diagnosis, resistance to therapy and lack of effective molecular biomarkers. Although previous research has examined the significance of genomic modifications, epigenetic modifications, and immune responses to define possible diagnostic and therapeutic targets, there is limited clinical translation of these results (31). The present study used an integrative strategy that consisted of bioinformatics, transcriptomic profiling, epigenetic analysis, immune infiltration evaluation, and molecular docking to provide further information on the molecular landscape of OSCC.

Table V. List of top 20 AREG inhibitors demonstrating binding affinity scores and hydrogen bond interactions.

Ligand	Binding affinity	Hydrogen bonds
Vinorelbine	-9.8	LYS-9
Docetaxel	-8.6	GLU-29, TYR-27, GLY-7, SER-6
Tipifarnib	-8.1	TYR-27
Tanespimycin	-8.1	GLU-32, TYR-27
AKT inhibitor VIII	-7.9	SER-5, GLU-15
AZ628	-7.8	GLN-39, GLN-40, CYS-38, TYR-42, GLY-44
A-770041	-7.7	HIS-22, LYS-26, ASN-10
S-Trityl-L-cysteine	-7.6	TYR-27
OSU-03012	-7.6	LYS-9, GLU-29
Nilotinib	-7.5	LYS-9, TYR-27
LY317615	-7.5	GLU-15, TYR-27
Etoposide	-7.5	ASN-10, ASN-13, CYS-25
GSK1904529A	-7.3	LYS-26
BMS-509744	-7.2	LYS-9, VAL-34
ERK5-IN-1	-7.2	GLN-17, CYS-25
PHA-665752	-7.2	ASN-13, CYS-12, CYS-25
Doramapimod	-7.1	SER-5, SER-6
FR-180204	-7.0	GLY-44, CYS-38, GLN-39
Cyclopamine	-7.0	TYR-27
BMS-708163	-7.0	GLU-32

Table VI. Comparative analysis of AREG- (25s)-neospirost-4-en-3-one and AREG-vinorelbine.

SN	RMSD (A˚)	Rg (A˚)	RMSF (nm)
AREG	5.33±0.03	33.59±0.002	3.15±0.29
(25s)-neospirost-4-en-3-one	1.17±0.001	4.79±0.001	0.41±0.04
Vinorelbine	3.40±0.01	5.35±0.001	2.27±0.10
AREG- (25s)-neospirost-4-en-3-one	7.61±0.04	33.64±0.002	3.76±0.27
AREG-vinorelbine	8.85±0.04	33.61±0.002	3.93±0.31

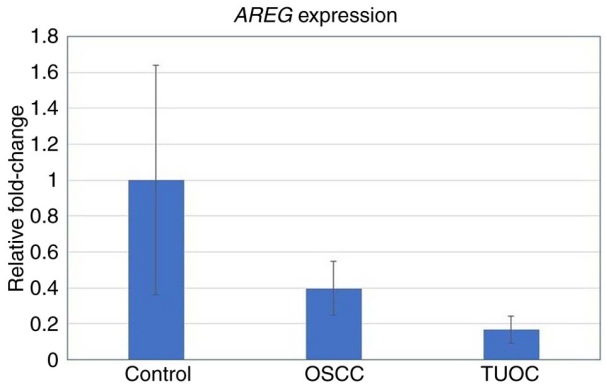

Figure 9. Expression levels of AREG in the controls, and in patients with resectable and technically unresectable oral cancer. Data are presented as the mean ± SEM.

Previous studies have reported frequently dysregulated genes in oral cancer, such as *TP53, EGFR, NOTCH1* and *CCND1* that are associated with proliferation, apoptosis and resistance to treatment (32,33). The present study demonstrated that *AREG* and *CX3CR1* were the most relevant genes associated with progressive OSCC, which are associated with immune infiltration and poor prognosis indicators. The clinical importance of AREG is further supported by a study conducted by Bourova-Flin *et al* (28), which reported that high expression of *AREG*, along with *Cyclin A1* and *DDX20/Gemin3*, was indicative of aggressive OSCC and correlated with unfavorable clinical outcomes. This reinforces the observation that *AREG* may contribute to tumor progression and immune-related changes in advanced disease. Equally, CX3CL1 has also been demonstrated to facilitate the migration and invasion of OSCC cells by increasing ICAM-1 expression via CX3CR1 receptor, which underscores its contribution to tumor invasiveness (34). These reports are consistent with the findings of the present study, in which *CX3CR1* expression was modulated in terms of immune cell invasion and disease severity. Collectively, these data support the notion that *AREG* and *CX3CR1* are potentially useful biomarkers to detect and describe OSCC

Table VII. Free binding energy of (25s)-neospirost-4-en-3-one and vinorelbine with AREG.

SN	Electrostatic energy (kcal/mol)	Vander Waals energy (kcal/mol)	Free binding energy of (ΔG) AREG-drug complex (kcal/mol)
(25s)-neospirost-4-en-3-one	-47.24±0.01 SEM	5.69±0.02 SEM	NA
Vinorelbine	105.55±0.03 SEM	33.40±0.03 SEM	NA
AREG	-351.46±1.59 SEM	-116.96±0.24 SEM	NA
AREG-(25s)-neospirost-4-en-3-one	-326.85±1.80 SEM	-115.10±0.25 SEM	+3.6
AREG-Vinorelbine	-400.60±2.26 SEM	-116.802±0.29 SEM	-15.26

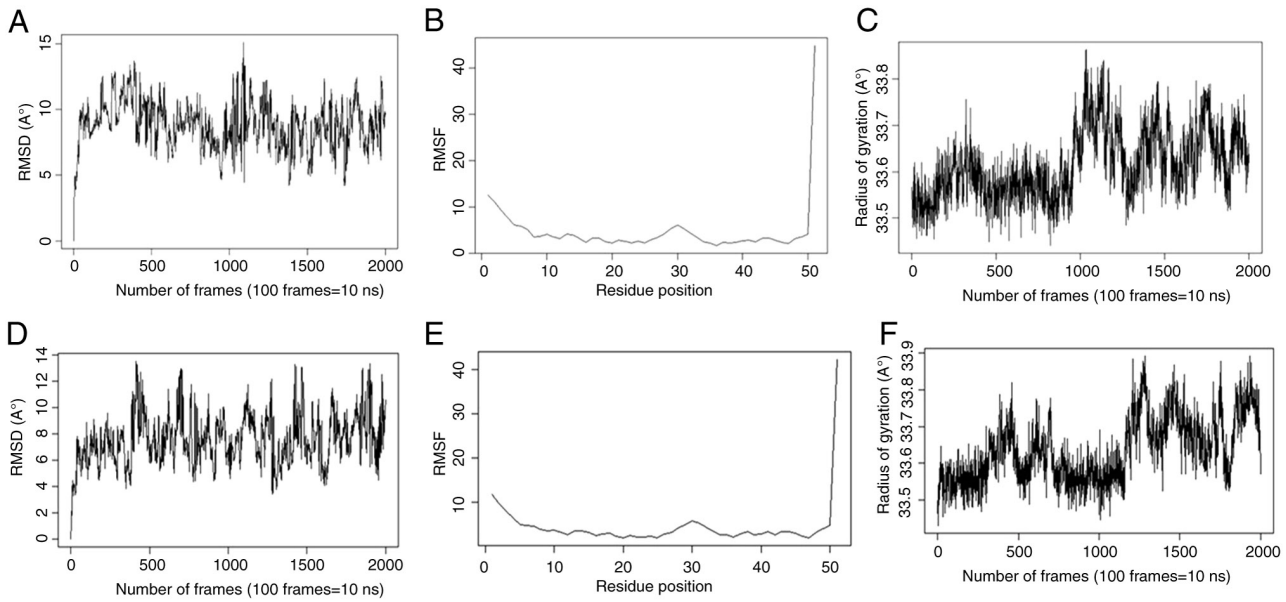

Figure 10. Molecular dynamics simulation demonstrating (A) RMSD, (B) RMSF, and (C) radius of gyration of vinorelbine - AREG complex. (D) RMSD, (E) RMSF, and (F) radius of gyration of AREG- (25s)-neospirost-4-en-3-one. RMSD, root mean square deviation; RMSF, root mean square fluctuation.

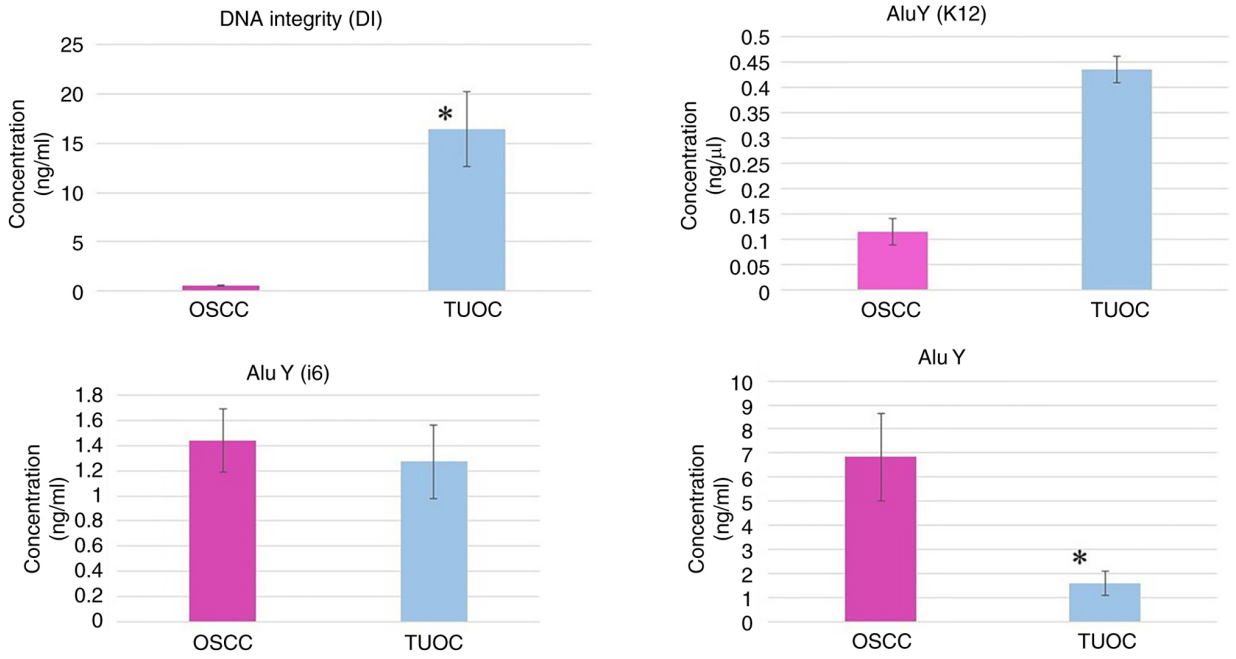

Figure 11. Comparison of Alu concentration in patients with resectable and technically unresectable oral cancer. Data are presented as the mean ± SEM. Statistical comparisons between the two groups were performed using an unpaired two-tailed Student's t-test. *P<0.05, vs. OSCC. OSCC, oral squamous cell carcinoma.

cases. Nonetheless, the diagnostic and prognostic ability of both genes seems to be limited as both of them showed only moderate AUC values (~0.6) in the ROC analyses. Thus, the results are to be considered as preliminary, and further research is required to confirm their applicability to clinical settings in larger patient groups.

The epigenetic modifications including CNVs and DNA methylation are the focus of OSCC development. In line with the earlier reports that reported promoter hypermethylation-induced silencing of tumor suppressors, such as *CDKN2A, DAPK1* and *MGMT* (35,36), the present study reported hypermethylation of *AREG* and *CX3CR1*, with certain CpG sites being associated with poor survival. CNV analysis identified deletions of *CX3CR1* that were associated with decreased expression, indicating its tumor-suppressive activity, whereas *AREG* was not affected by deletion of CNV, indicating further epigenetic or post-transcriptional regulation. On the immunological front, previous research has linked $CD8^+$ T-cell infiltration with improved prognosis, and increased Tregs or MDSCs with poorer outcomes (37,38). The present study demonstrated that *AREG* and *CX3CR1* were associated with $CD8^+$ T-cells and neutrophils and $CD4^+$ T-cells respectively, which indicated differential roles in immune modulation. Taken together, these results support previous data of chemokine and growth factor implication by modulating tumor microenvironment in OSCC and emphasize their role in the regulation of the epigenome, as well as tumor-immune interactions (39,40).

In a previous study on non-small cell lung cancer and HNSCC, changes in serum levels of EGFR and its ligands, such as *AREG*, were described, and lower levels of *AREG* expression were found in serum samples of patients (41). These findings are in line with the findings of the present study, which also revealed the reduced expression of *AREG* in the blood of patients with TUOC. Although the present study was not able to do tissue-level validation, several previous studies have established that *AREG* is overexpressed in OSCC tissues (28,29,42,43). This, along with the observation of lower *AREG* levels in circulation in the present study, confirms the hypothesis of the 'dual faces', in which local tumor upregulation is accompanied by lower systemic levels. These findings also indicate that local tumor expression can be more useful in prognosis compared to circulating levels. *CX3CR1* was, however, not detectable in serum samples, presumably due to very low levels of expression or degradation, suggesting that tissue-based analysis can be more informative on this marker.

Transposable elements, particularly Alu elements, are critical in the progression of cancer (44). Consistent with previous studies, the present study also discovered that the DNA integrity ratio (Alu115/Alu247) was significantly higher in patients with TUOC and indicated more genomic instability (45,46). Whereas AluY (K12) expression was more elevated in TUOC, the total expression of the AluY family was more elevated in resectable OSCC, indicating stage-specific roles of Alu subfamilies. The results are in line with previous research demonstrating that some Alu subfamilies differ in expression across cancer types, which supports their possible use as biomarkers of disease staging and monitoring (45).

Due to the drawbacks of traditional OSCC therapy, natural compounds have become the focus of interest as possible anticancer agents as they can regulate oxidative stress, inflammation and apoptosis pathways (47,48). The present study identified 274 drug-like compounds; however, only vinorelbine, an approved drug, exhibited a strong and stable binding with AREG in molecular docking and molecular dynamics simulations. These results suggest that vinorelbine has a higher therapeutic potential compared to the identified natural compounds. Although limited by a small validation cohort and reliance on bioinformatics data, the results are exploratory and indicate that *AREG, CX3CR1* and Alu elements can be considered as a potential therapeutic targets and biomarkers in OSCC. To validate these findings and enhance biomarker-based treatment strategies, larger, multi-center and functional studies are required.

Overall, the analyses of genomic, epigenetic, immunological and transposable elements were combined in the present study to identify novel biomarkers and therapeutic targets in OSCC. The results enhance the current understanding of the molecular mechanisms of OSCC and may be applied to designing the individual treatment plans in accordance with the profile of biomarkers.

Acknowledgements

Not applicable.

Funding

The present study was supported by the intramural funding from Parul University, Vadodara, India (grant no. RDC/IMSL/213).

Availability of data and materials

The data generated in the present study may be requested from the corresponding author.

Authors' contributions

All authors (NK, CJ, MP and RG) contributed to the conception and design of the study. Material preparation, data collection and analysis were performed by NK and CJ. Molecular dynamics simulation and qPCR were performed by MP. NK and RG confirm the authenticity of all the raw data. The first draft of the manuscript, editing and supervision was performed by RG, and all authors commented on previous versions of the manuscript. All authors have read and approved the final manuscript.

Ethics approval and consent to participate

The study protocol was reviewed and approved by the Ethics Committee of Parul University (Approval no. PUIECHR/PIMSR/00/081734/5307) and was conducted in accordance with institutional ethical standards and regulatory guidelines. All patients signed an informed consent form, and all procedures performed in this study were in accordance with the principles for medical research of the 1964 Declaration of Helsinki and its later amendments or comparable ethical standards.

Patient consent for publication

Not applicable.

Competing interests

The authors declare that they have no competing interests.

References

1. Bray F, Laversanne M, Sung H, Ferlay J, Siegel RL, Soerjomataram I and Jemal A: Global cancer statistics 2022: GLOBOCAN estimates of incidence and mortality worldwide for 36 cancers in 185 countries. CA Cancer J Clin 74: 229-263, 2024.
2. Shimojukkoku Y, Nguyen PT, Ishihata K, Ishida T, Kajiya Y, Oku Y, Kawaguchi K, Tsuchiyama T, Saijo H, Shima K and Sasahira T: Role of early growth response-1 as a tumor suppressor in oral squamous cell carcinoma. Discov Oncol 15: 714, 2014.
3. Kijowska J, Grzegorczyk J, Gliwa K, Jędras A and Sitarz M: Epidemiology, diagnostics, and therapy of oral cancer-update review. Cancers (Basel) 16: 3156, 2024.
4. Yosefof E, Edri N, Kurman N, Bachar G, Shpitzer T, Mizrachi A and Popovtzer A: The role of adjuvant radiotherapy for early-stage oral cavity cancer with minor adverse features; A single institute experience. Head Neck 47: 1839-1847, 2025.
5. Caputo WL, de Souza MC, Basso CR, Pedrosa VA and Seiva FRF: Comprehensive profiling and therapeutic insights into differentially expressed genes in hepatocellular carcinoma. Cancers (Basel) 15: 5653, 2023.
6. Zakari S, Niels NK, Olagunju GV, Nnaji PC, Ogunniyi O, Tebamifor M, Israel EN, Atawodi SE and Ogunlana OO: Emerging biomarkers for non-invasive diagnosis and treatment of cancer: A systematic review. Front Oncol 4: 1405267, 2024.
7. Ye M, Huang X, Wu Q and Liu F: Senescent stromal cells in the tumor microenvironment: Victims or accomplices? Cancers (Basel) 15: 1927, 2023.
8. Lakshminarasimhan R and Liang G: The role of DNA methylation in cancer. Adv Exp Med Biol 945: 151-172, 2016.
9. Yi L, Wu G, Guo L, Zou X and Huang P: Comprehensive analysis of the PD-L1 and immune infiltrates of m6A RNA methylation regulators in head and neck squamous cell carcinoma. Mol Ther Nucleic Acids 21: 299-314, 2020.
10. Jiang Y, Zong W, Ju S, Jing R and Cui M: Promising member of the short interspersed nuclear elements (Alu elements): Mechanisms and clinical applications in human cancers. J Med Genet 56: 639-645, 2019.
11. Chen LL and Yang L: ALUternative regulation for gene expression. Trends Cell Biol 27: 480-490, 2017.
12. Masson E, Maestri S, Bordeau V, Cooper DN, Férec C and Chen JM: Alu insertion-mediated dsRNA structure formation with pre-existing Alu elements as a disease-causing mechanism. Am J Hum Genet 111: 2176-2189, 2024.
13. Wang ZY, Ge LP, Ouyang Y, Jin X and Jiang YZ: Targeting transposable elements in cancer: Developments and opportunities. Biochim Biophys Acta Rev Cancer 1879: 189143, 2024.
14. Lehle S, Emons J, Hack CC, Heindl F, Hein A, Preuß C, Seitz K, Zahn AL, Beckmann MW, Fasching PA, *et al*: Evaluation of automated techniques for extraction of circulating cell-free DNA for implementation in standardized high-throughput workflows. Sci Rep 13: 373, 2023.
15. Choudhari AS, Mandave PC, Deshpande M, Ranjekar P and Prakash O: Phytochemicals in cancer treatment: From preclinical studies to clinical practice. Front Pharmacol 10: 1614, 2020.
16. Othman B, Beigh S, Albanghali MA, Sindi AAA, Shanawaz MA, Ibahim MAEM, Marghani D, Kofiah Y, Iqbal N and Rashid H: Comprehensive pharmacokinetic profiling and molecular docking analysis of natural bioactive compounds targeting oncogenic biomarkers in breast cancer. Sci Rep 15: 5426, 2025.
17. Patel MS, Sinngh P, Gandupalli L and Gupta R: Identification and evaluation of survival-associated common chemoresistant genes in cancer. Biomed Biotechnol Res J 8: 320-327, 2024.
18. Tang Z, Li C, Kang B, Gao G, Li C and Zhang Z: GEPIA: A web server for cancer and normal gene expression profiling and interactive analyses. Nucleic Acids Res 45(W1): W98-W102, 2017.
19. Tang Z, Kang B, Li C, Chen T and Zhang Z: GEPIA2: An enhanced web server for large-scale expression profiling and interactive analysis. Nucleic Acids Res 47(W1): W556-W560, 2019.
20. Gu Z, Eils R and Schlesner M: Complex heatmaps reveal patterns and correlations in multidimensional genomic data. Bioinformatics 32: 2847-2849, 2016.
21. Liao Y, Wang J, Jaehnig EJ, Shi Z and Zhang B: WebGestalt 2019: Gene set analysis toolkit with revamped UIs and APIs. Nucleic Acids Res 47(W1): W199-W205, 2019.
22. Modhukur V, Iljasenko T, Metsalu T, Lokk K, Laisk-Podar T and Vilo J: MethSurv: A web tool to perform multivariable survival analysis using DNA methylation data. Epigenomics 10: 277-288, 2018.
23. Li T, Fu J, Zeng Z, Cohen D, Li J, Chen Q, Li B and Liu XS: TIMER2.0 for analysis of tumor-infiltrating immune cells. Nucleic Acids Res 48(W1): W509-W514, 2020.
24. Kingsley JP, Pranay G, Priya A and Chandrakumar MJ: Human papilloma virus testing in oral squamous cell carcinoma in Southern India: A case-control study. Current Medical Issues 19: 12-18, 2021.
25. Livak KJ and Schmittgen TD: Analysis of relative gene expression data using real-time quantitative PCR and the 2(-Delta Delta C(T)) Method. Methods 25: 402-408, 2001.
26. Hubley R, Finn RD, Clements J, Eddy SR, Jones TA, Bao W, Smit AF and Wheeler TJ: The Dfam database of repetitive DNA families. Nucleic Acids Res 44(D1): D81-D89, 2016.
27. Dallakyan S and Olson AJ: Small-molecule library screening by docking with PyRx. Methods Mol Biol 1263: 243-250, 2015.
28. Bourova-Flin E, Derakhshan S, Goudarzi A, Wang T, Vitte AL, Chuffart F, Khochbin S, Rousseaux S and Aminishakib P: The combined detection of Amphiregulin, Cyclin A1 and DDX20/Gemin3 expression predicts aggressive forms of oral squamous cell carcinoma. Br J Cancer 125: 1122-1134, 2021.
29. Gao J, Ulekleiv CH and Halstensen TS: Epidermal growth factor (EGF) receptor-ligand based molecular staging predicts prognosis in head and neck squamous cell carcinoma partly due to deregulated EGF-induced amphiregulin expression. J Exp Clin Cancer Res 35: 151, 2016.
30. He C, Wu Y, Nan X, Zhang W, Luo Y, Wang H, Li M, Liu C, Liu J, Mou X and Liu Y: Induction of CX3CL1 expression by LPS and its impact on invasion and migration in oral squamous cell carcinoma. Front Cell Dev Biol 12: 1371323, 2024.
31. Ravindran S, Ranganathan S, R K, J N, A S, Kannan SK, Prasad K D, Marri J and K R: The role of molecular biomarkers in the diagnosis, prognosis, and treatment stratification of oral squamous cell carcinoma: A comprehensive review. J Liq Biopsy 7: 100285, 2025.
32. Kunesch K: GATA3-expressing regulatory T cells accumulate in response to early cancerous changes via TCR-dependent local proliferation: Dissertation, RWTH Aachen University, 2024.
33. Gintoni I, Vassiliou S, Chrousos GP and Yapijakis C: Review of disease-specific microRNAs by strategically bridging genetics and epigenetics in oral squamous cell carcinoma. Genes (Basel) 14: 1578, 2023.
34. Wu CY, Peng PW, Renn TY, Lee CJ, Chang TM, Wei AI and Liu JF: CX3CL1 induces cell migration and invasion through ICAM-1 expression in oral squamous cell carcinoma cells. J Cell Mol Med 27: 1509-1522, 2023.
35. Izumi T, Rychahou P, Chen L, Smith MH and Valentino J: Copy number variation that influences the ionizing radiation sensitivity of oral squamous cell carcinoma. Cells 12: 2425, 2023.
36. Agarwal N and Jha AK: DNA hypermethylation of tumor suppressor genes among oral squamous cell carcinoma patients: A prominent diagnostic biomarker. Mol Biol Rep 52: 44, 2024.
37. Kondoh N and Mizuno-Kamiya M: The role of immune modulatory cytokines in the tumor microenvironments of head and neck squamous cell carcinomas. Cancers (Basel) 14: 2884, 2022.
38. Fu C and Jiang A: Dendritic cells and CD8 T cell immunity in tumor microenvironment. Front Immunol 9: 3059, 2018.
39. Sahingur SE and Yeudall WA: Chemokine function in periodontal disease and oral cavity cancer. Front Immunol 6: 214, 2015.
40. Mesgari H, Esmaelian S, Nasiri K, Ghasemzadeh S, Doroudgar P and Payandeh Z: Epigenetic regulation in oral squamous cell carcinoma microenvironment: A comprehensive review. Cancers (Basel) 15: 5600, 2023.

41. Lemos-Gonzalez Y, Rodríguez-Berrocal FJ, Cordero OJ, Gómez C and Páez de la Cadena M: Alteration of the serum levels of the epidermal growth factor receptor and its ligands in patients with non-small cell lung cancer and head and neck carcinoma. Br J Cancer 96: 1569-1578, 2007.
42. Li M, Wei Y, Huang W, Wang C, He S, Bi S, Hu S, You L and Huang X: Identifying prognostic biomarkers in oral squamous cell carcinoma: An integrated single-cell and bulk RNA sequencing study on mitophagy-related genes. Sci Rep 14: 19992, 2024.
43. Zhou J, Xu Y, Li Y, Zhang Q, Zhong L, Pan W, Ji K, Zhang S, Chen Z, Liu Y, *et al*: Cancer-associated fibroblasts derived amphiregulin promotes HNSCC progression and drug resistance of EGFR inhibitor. Cancer Lett 622: 217710, 2025.
44. Park MK, Lee JC, Lee JW and Hwang SJ: Alu cell-free DNA concentration, Alu index, and LINE-1 hypomethylation as a cancer predictor. Clin Biochem 94: 67-73, 2021.
45. Nair MG, Ramesh RS, Naidu CM, Mavatkar AD, V P S, Ramamurthy V, Somashekaraiah VM, C E A, Raghunathan K, Panigrahi A, *et al*: Estimation of ALU repetitive elements in plasma as a cost-effective liquid biopsy tool for disease prognosis in breast cancer. Cancers (Basel) 15: 1054, 2023.
46. Lehner J, Stötzer OJ, Fersching D, Nagel D and Holdenrieder S: Circulating plasma DNA and DNA integrity in breast cancer patients undergoing neoadjuvant chemotherapy. Clin Chim Acta 425: 206-211, 2013.
47. Farhan M: Revisiting the antioxidant-prooxidant conundrum in cancer research. Med Oncol 41: 179, 2024.
48. Huang J, Xu Y, Wang Y, Su Z, Li T, Wu S, Mao Y, Zhang S, Weng X and Yuan Y: Advances in the study of exosomes as drug delivery systems for bone-related diseases. Pharmaceutics 15: 220, 2023.